Neuroscience Letters 514 (2012) 35–41

Contents lists available at SciVerse ScienceDirect

Neuroscience Letters

journal homepage: www.elsevier.com/locate/neulet

Cortical brain imaging by adaptive filtering of NIRS signals

Muhammad Aqil[a,1], Keum-Shik Hong[a,b,*], Myung-Yung Jeong[a,1], Shuzhi Sam Ge[a,c,1]

[a] Department of Cogno-Mechatronics Engineering, Pusan National University, 30 Jangjeon-dong, Geumjeong-gu, Busan 609-735, Republic of Korea
[b] School of Mechanical Engineering, Pusan National University, 30 Jangjeon-dong, Geumjeong-gu, Busan 609-735, Republic of Korea
[c] Department of Electrical and Computer Engineering, National University of Singapore, Singapore 117576, Singapore

ARTICLE INFO

Article history:
Received 28 November 2011
Received in revised form 9 February 2012
Accepted 14 February 2012

Keywords:
Functional near-infrared spectroscopy
General linear model
Optical brain imaging
Real-time mapping
Recursive least square estimation
Statistical parametric mapping

ABSTRACT

This paper presents an online brain imaging framework for cognitive tasks conducted with functional near-infrared spectroscopy (fNIRS). The measured signal at each channel is regarded as the output from a linear system with unknown coefficients. The unknown coefficients are estimated by using the recursive least squares estimation (RLSE) method. The validity of the estimated parameters is tested using the *t*-statistics. Contrary to the classical approach that is offline and applies the same preprocessing scheme to all channels, the proposed RLSE method for a linear model formulation provides an independent robust adaptive process for individual channels. The experiments carried out with two fNIRS instruments (continuous-wave and frequency-domain) have verified the potential of the proposed methodology which can facilitate a prompt medical diagnostics by providing real-time brain activation maps.

1. Introduction

Functional near-infrared spectroscopy (fNIRS) is a non-invasive probing technology for brain-activity monitoring, which measures the absorbed quantity of near-infrared light of 650–950 nm wavelength [1,4–6,8,13–15,20–22,24,25]. By measuring diffusely scattered lights, fNIRS enables determination of the concentration changes of oxy-hemoglobin (HbO) and deoxy-hemoglobin (HbR) in the targeted brain areas [14,15]. This technique has been applied to the study of numerous brain systems under several clinical conditions, see [5,15,21,24]. For brain computer interface, fNIRS offers advantages over functional magnetic resonance imaging (fMRI); specifically in its low dimensional data that allows fast processing, portability, cost efficiency, and good temporal resolution [5]. Furthermore, it is superior to electroencephalography (EEG) in spatial resolution and signal-to-noise ratio (SNR).

However, a drawback of fNIRS is the lack of provision of anatomical information, making localization of the brain area difficult [11,18]. This problem was addressed in [25] and the use of a 3D digitizer to localize the fNIRS signal in the cerebral cortex on top of an anatomical image of fMRI was presented. Another drawback of fNIRS is its limited penetration depth due to the high level of light scattering within tissues. Since the specific utility proposed in this paper focuses on the cortical region of the brain, this disadvantage of fNIRS relative to fMRI can be disregarded.

Currently, many research groups are developing statistical-analysis toolboxes emphasizing the parametric approach of the general linear model (GLM) [14,20,25]. The GLM is a statistical linear model that explains data as a linear combination of explanatory variables with an additive noise [1,5,7,9,14,16,20,25]. As the GLM measures the temporal variation pattern of signals rather than their absolute magnitude, it is robust in many cases, even in the cases of incorrect differential path length factors (DPF) and severe optical signal attenuation [25]. The event-related paradigm in [20] showed that the parametric approach can provide a statistically powerful solution to brain activation mapping. Before processing the data for activation detection using statistical analysis, preprocessing of the measured signals is usually performed to improve the SNR. Important preprocessing steps include filtering of particular frequency band(s), baseline correction, detrending of low-frequency signals as well as pre-whitening and pre-coloring [5,7,25]. Furthermore, preprocessing is mostly performed according to a generalized scenario and no special attention is paid to individual channels separately (i.e., some channels may require different preprocessing parameters).

There are limitations and conditions in the course of real-time brain imaging as pointed out by other researchers, see [23] and references therein. The possibility of detecting a fast optical response was demonstrated in [6,13], but with an extensive offline processing (via averaging of several sessions of a particular task) because of the too weak signals. Studies on a matrix-based template were also pursued in the capacity of brain mapping to provide

* Corresponding author at: Department of Cogno-Mechatronics Engineering, Pusan National University, 30 Jangjeon-dong, Geumjeong-gu, Busan 609-735, Republic of Korea. Tel.: +82 51 510 2973/2454; fax: +82 51 514 0685.
E-mail addresses: aqil@pusan.ac.kr (M. Aqil), kshong@pusan.ac.kr (K.-S. Hong), myjeong@pusan.ac.kr (M.-Y. Jeong), samge@nus.edu.sg (S.S. Ge).
[1] Tel.: +82 51 510 2973; fax: +82 51 514 0685.

0304-3940/$ – see front matter © 2012 Elsevier Ireland Ltd. All rights reserved.
doi:10.1016/j.neulet.2012.02.048

signal-strengths of the measuring channels [1,14], in which prior assumptions on the process and observation noise distributions were the main drawback of such Kalman filter-based studies. The assessment of noise distributions was done prior to experiments, which requires some expectation of the inter-trial variability of the response.

Taking inspiration from the recursive least squares estimation (RLSE) filter's adaptability, fast convergence and run-time adjustment to varying input statistics [10,17], the present study develops an RLSE-based framework for online cortical brain imaging. The measured signal at each channel is regarded as the output from a linear system with unknown but adaptable coefficients [2,12]. The unknown coefficients are estimated by using the RLSE method. The process is not bounded to an initial guess or to tuning of critical parameters. Two different domain NIRS instruments, continuous-wave (CW) and frequency domain (FD), are utilized to validate the proposed scheme. The method is further verified by utilizing the experimental data provided by the authors of [25]. The proposed online brain imaging framework offers a quick medical diagnostics facility. Also, it has a great potential to work equally well for parametric fMRI imaging.

The following are the main contributions of the present study. (i) A run-time interpolated *t*-mapping-based brain imaging framework for fNIRS technology is proposed for the first time. (ii) An adaptive RLSE-based methodology is derived for activity strength estimation. (iii) Owing to its parametric structure, the scheme acts as an adaptive spatial filter besides an estimator of the activity strength. (iv) The proposed adaptive parametric-filtering is particularly attractive for its obviation of any kind of preprocessing including low-pass and high-pass filtering, baseline specification, detrending, and pre-whitening and/or pre-coloring. (v) Contrary to the classical approaches (mostly offline), the proposed adaptive processing provides an online robust treatment at each measuring channel unanimously as per the channel's requirement.

2. Theory

2.1. Signal conditioning

The concentration change of HbX (i.e., HbO and HbR), Δc_{HbX} in μM, using the modified Beer–Lambert law (MBLL) [4] is given by

$$\begin{bmatrix} \Delta\phi^i_{\mathrm{HbO}}(t) \\ \Delta\phi^i_{\mathrm{HbR}}(t) \end{bmatrix} = \begin{bmatrix} a_{\mathrm{HbO}}(\lambda_1) & a_{\mathrm{HbR}}(\lambda_1) \\ a_{\mathrm{HbO}}(\lambda_2) & a_{\mathrm{HbR}}(\lambda_2) \end{bmatrix}^{-1} \begin{bmatrix} \Delta\phi^i(t;\lambda_1) \\ \Delta\phi^i(t;\lambda_2) \end{bmatrix}, \quad (1)$$

$$\Delta c^i_{\mathrm{HbX}}(t) = \frac{\Delta\phi^i_{\mathrm{HbX}}(t)}{d^i l^i}, \quad (2)$$

where the superscript i ($i = 1, 2, \ldots, M$) denotes the ith measuring channel of the source and detector pair, M denotes the total number of channels, $\Delta\phi^i_{\mathrm{HbX}}(t)$ is the optical density variation of HbX in μM mm at the ith channel, $\Delta\phi^i(t;\lambda_j)$ ($j = 1, 2$) is the unitless total optical density variation of the light source of wavelength λ_j, $a_{\mathrm{HbX}}(\lambda_j)$ is the extinction coefficient of HbX in $\mu\mathrm{M}^{-1}\,\mathrm{mm}^{-1}$, d^i is the unitless DPF, and l^i is the distance (in millimeters) between the source and the detector at the ith channel. Besides the applicability of the MBLL (1)-(2) to CW- and FD-NIRS systems, it is worth noting that FD-NIRS provides concentration of HbX on the absolute scale by means of solving Boltzmann's transport equation [8].

The existing ambiguities of exact activity localization due to the irregular and distant optodes (co-located source-detector) can be coped with a first-order Rytov approximation [19,25]. The interpolated value of the HbX changes at location r is given by

$$\Delta c_{\mathrm{HbX}}(t, r) = \sum_{i=1}^{M} b^i(r)\Delta\phi^i_{\mathrm{HbX}}(t), \quad (3)$$

where $b^i(r)$ corresponds to the interpolation kernel derived from the diffusion equation (i.e., the spatial correlation with the adjacent channels' hemoglobin status) [3]. Due to the interpolation relationship in (3), the statistical testing of $\Delta c_{\mathrm{HbX}}(t, r)$ can be directly transferred from the statistical testing of $\Delta\phi^i_{\mathrm{HbX}}(t)$. This will be discussed in Section 2.5.

2.2. Brain activity model

In this section, a linear model to identify the activation spot(s) for a cognitive task is introduced. For $y^i(t) \triangleq \Delta\phi^i_{\mathrm{HbX}}(t)$, the discrete form of the model is defined as

$$\begin{aligned} y^i(k) &= x_1(k)\beta^i_1(k) + x_2(k)\beta^i_2(k) + x_3(k)\beta^i_3(k) + 1\cdot\beta^i_4(k) + \varepsilon^i(k) \\ &= X^T(k)\beta^i(k) + \varepsilon^i(k), \end{aligned} \quad (4)$$

where k is the discrete time, $X(k) \in \Re^{4\times 1}$ is the regression vector at the kth sampling time, superscript T is the transpose operator, $\beta^i(k) = [\,\beta^i_1(k) \;\; \beta^i_2(k) \;\; \beta^i_3(k) \;\; \beta^i_4(k)\,]^T$ is the slowly varying parameters representing the activity strengths at channel i, and $\varepsilon^i \in \Re$ denotes the zero-mean Gaussian noise at channel i. Now, for run-time realization, the activity parameter vector $\beta^i(k)$ needs to be found at each time step k.

In this paper, the regression vector $X(k)$ is considered to (but not restricted to) consist of four components: the basis function $x_1(k)$ (i.e., the expected hemodynamic response obtained by convolving the canonical hemodynamic HbO response function with the experimental box-car function), its two derivatives $x_2(k) = \Delta x_1(k)$ and $x_3(k) = \Delta^2 x_1(k)$, and an offset, see how the design matrix in [25] is formed. It is assumed that the proposed activity regressor $X(k)$ is uncorrelated with disturbances in the measured signal.

2.3. Adaptive recursive least squares estimation

The RLSE filter computes the temporal statistics directly at each time step to determine the optimal coefficients [10,17]. The single-channel model defined in (4) converts the finding of the optimal estimated parameter $\hat{\beta}^i$ into the minimization of the cost-function

$$V(\hat{\beta}^i, k) = \frac{1}{2}\sum_{j=1}^{k}(e^i(j))^2, \quad (5)$$

where the estimation error is defined as

$$e^i(k) = y^i(k) - X^T(k)\hat{\beta}^i(k-1). \quad (6)$$

Solving the minimization problem, the RLSE [10,17] is given by

$$\hat{\beta}^i(k) = \hat{\beta}^i(k-1) + K(k)e^i(k), \quad (7)$$

$$K(k) = P(k-1)X(k)(1 + X^T(k)P(k-1)X(k))^{-1}, \quad (8)$$

$$P(k) = (I - K(k)X^T(k))P(k-1), \quad (9)$$

where $K(k) \in \Re^{4\times 1}$ is the weighting vector for parameter updating and $P(k) \in \Re^{4\times 4}$ is the recursive inverse of the input covariance matrix at sample time k. The initial value $P(k-1)$ is chosen to be δI, $\delta = 10$, see [10].

2.4. Robustness of RLSE scheme

In the presence of a precise and consistently exciting prediction function $X(k)$, the RLSE algorithm can be robust if it is implemented on a stable dynamical system [10]. For the problem in hand, the robustness of the RLSE algorithm can be analyzed quantitatively by investigating the statistical variance (*Var*) of the estimated

activity parameter $\hat{\beta}^i(k)$, perturbed by the disturbances $\delta y^i(k)$ in the measured signal $y^i(k)$, at channel i as

$$Var[\hat{\beta}^i(k)] = E[\hat{\beta}^i(k)]^2 - [E\{\beta^i(k)\}]^2, \quad (10)$$

where $E[\beta^i(k)]$ is the mean value (supposed to be the actual activity value). Utilizing (7) with (6) for the perturbed signal $y^i(k) + \delta y^i(k)$, we obtain

$$Var[\hat{\beta}^i(k)] = 2\beta^i(k)E[K(k)\delta y^i(k)] + E[K^2(k)\{\delta y^i(k)\}^2] \quad (11)$$

Apparently from (8) to (9), the disturbances that are uncorrelated with $X(k)$ are also uncorrelated with $K(k)$. Thus, we conclude that $\lim_{k\to\infty} E[K(k)\delta y^i(k)] = 0$ and the RLSE-based estimation is robust against all the uncorrelated disturbances.

2.5. Activation mapping

The activity strength at any location r over the full range of optodes can be found by using $\hat{\beta}(k)$ from all the channels, where

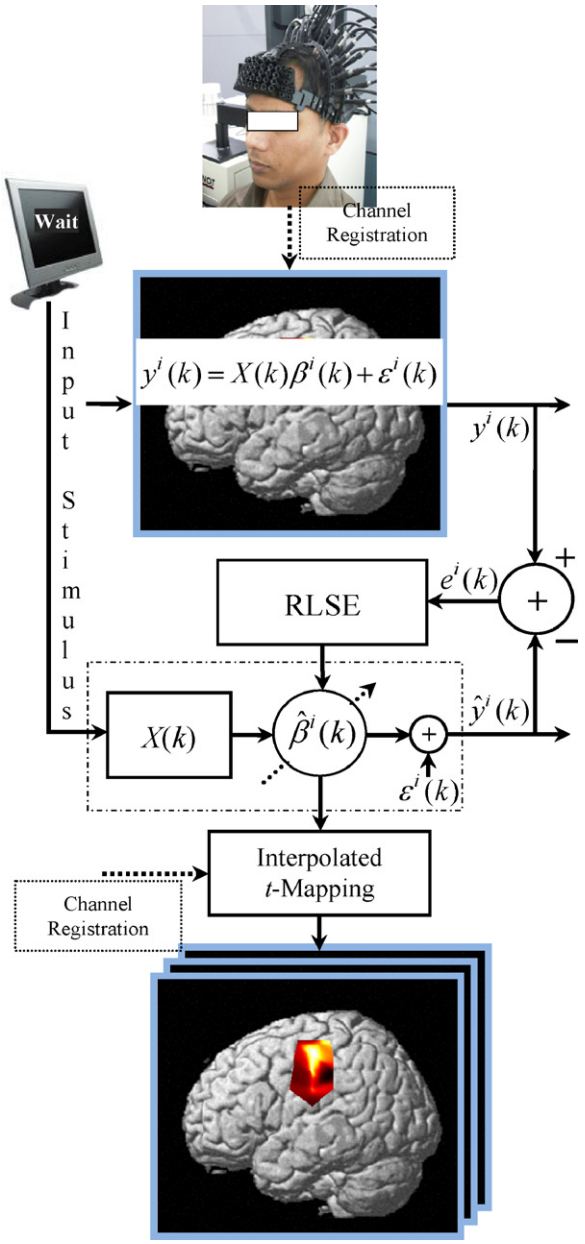

Fig. 1. Schematic diagram of the proposed RLSE-based brain-imaging framework.

$\hat{\beta}(k)$ is the stacking form of $\hat{\beta}^i(k)$. As done offline in [25], the interpolated activity strength $\hat{\alpha}(k, r)$ at time k is obtained as

$$\hat{\alpha}(k, r) = (B^T(r) \otimes I_4)\hat{\beta}(k) \quad (12)$$

where $B(r)$ is the stacking vector of interpolation kernels given by

$$B(r) = [\, b^1(r) \quad b^2(r) \quad \cdots \quad b^M(r)\,] \quad (13)$$

and $\otimes$ is the Kronecker product. The corresponding error covariance is

$$C_{\hat{\alpha}}(k, r) = (B^T(r)\Sigma B(r)) \otimes (X^+ \Lambda X^{+T}), \quad (14)$$

where $\Sigma = diag(\sigma_1^2, \sigma_2^2, \cdots, \sigma_M^2)$ with σ_i^2 being the variance at channel i, the superscript + denotes the pseudo inverse operator, X is the stacking form of the regressor vector $X(k)$, and Λ is the common temporal correlation matrix for all the channels. It is worth mentioning that smoothening, pre-whitening, or pre-coloring are neither used nor required by the proposed adaptive approach; that is, $\Lambda = I$. The response of the signal of interest at each sample time k can be calculated using an inner product with a contrast vector $c \in \Re^{4\times 1}$ as

$$\hat{\chi}(k, r) = c^T \hat{\alpha}(k, r). \quad (15)$$

The corresponding error covariance is given by

$$C_{\hat{\chi}}(k, r) = (B^T(r)\Sigma B(r)) \otimes (c^T \boldsymbol{X}^+ \Lambda \boldsymbol{X}^{+T} c). \quad (16)$$

Under the null hypothesis, the response signal $\hat{\chi}(k, r)$ is distributed in the following zero-mean Gaussian distribution

$$\hat{\chi}(r, k) : N(0, C_{\hat{\chi}}(r)). \quad (17)$$

Hence, the corresponding t-statistics is given by

$$T(r, k) = \frac{c^T \hat{\alpha}(r, k)}{\sqrt{(B^T(r)\Sigma B(r))(c^T \boldsymbol{X}^+ \Lambda \boldsymbol{X}^{+T} c)}}, \quad (18)$$

where T is the estimated t-value at location r. Thus, the interpolated t-statistics based brain activation map over the full range of the measuring optodes can be drawn on a brain template.

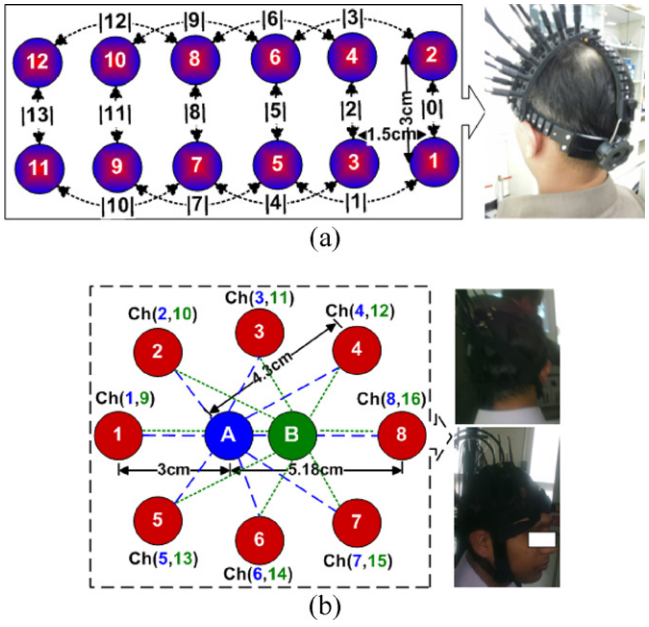

Fig. 2. Channel configurations covering the primary left motor cortex: (a) DYNOT holder cap measuring 14 channels with 12 optodes and (b) Imagent's sensor pad measuring 16 channels with 8 sources and dual-distance detectors A and B.

3. Method

Fig. 1 illustrates the schematic of the proposed RLSE-based real-time brain imaging framework. Fig. 2(a) shows the channel configuration of the CW-NIRS instrument (DYNOT, NIRx Medical Technologies). The system is configured to provide dual wavelength measurements (760 nm and 830 nm) from fourteen channels with a sampling frequency of 1.81 Hz. Fig. 2(b) shows the channel configuration of the two-wavelength (690 nm and 830 nm) FD-NIRS instrument (Imagent; ISS, Inc.) measuring sixteen channels at a sampling rate of 15.6250 Hz.

The left-motor-cortex-targeting physiological experiment is based on the right-index-finger-tapping (RIFT) task. Since the target area of the finger-tapping task is within the primary motor cortex, the activation occurs within the limits of the penetration depth of the NIRS instruments. The specific behavioral protocol of the experiment is the following. An initial 20 s for signal equilibrium followed by three sessions each of 40 s, including 20 s for the

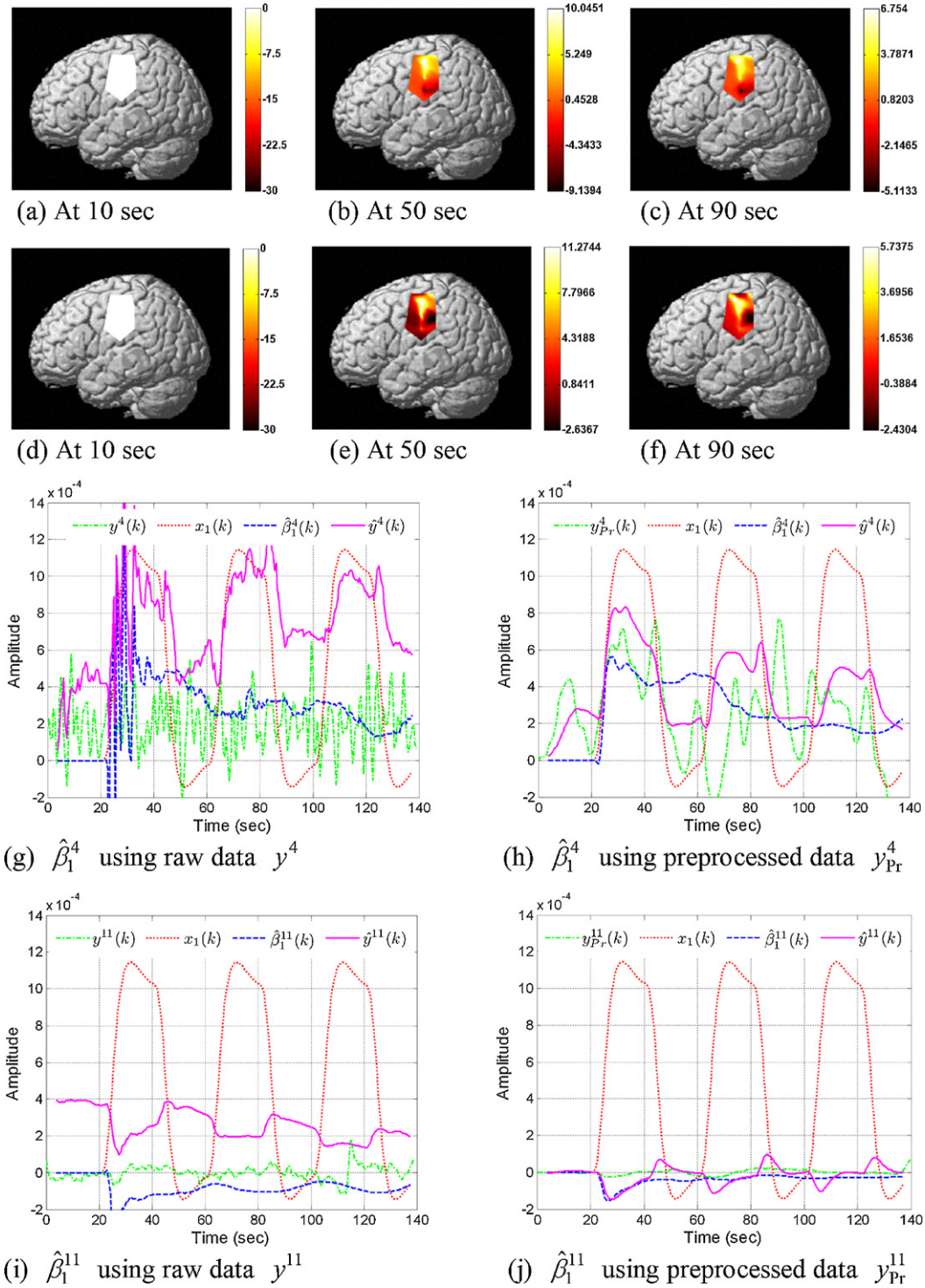

Fig. 3. Results with DYNOT: (a)–(c) online brain activation maps obtained using raw data, (d)–(f) offline brain activation maps obtained using preprocessed data, (g) and (h) parameter convergence in an active channel (Ch. 4) (raw vs. preprocessed), and (i) and (j) parameter convergence in an inactive channel (Ch. 11) (raw vs. preprocessed).

RIFT task and 20 s for rest. The total experiment time takes 140 s. The validation experiments are conducted twice with both CW- and FD-NIRS instruments for 5 healthy male subjects of age 28 ± 3 years.

4. Results

Fig. 3(a)–(c) shows the online brain activation maps, using the DYNOT probing instrument and its raw data, at three time instants 10, 50, and 90 s, respectively. On the other hand, Fig. 3(d)–(f) depicts the brain activation maps obtained by using the preprocessed data. In the second case, the DYNOT signals were recorded first, and preprocessed with a low-pass Gaussian filter and detrended with wavelet transform before inputting to the RLSE scheme. The comparison of Fig. 3(a)–(c) and (d)–(f) demonstrates that almost identical activity maps are achieved in both cases, which reveals that the RLSE approach is robust in the presence of disturbances and noises. For further validation, the convergence of parameter $\hat{\beta}_1^i$ and the estimated output $\hat{y}^i$ along with the utilized data (raw data y^i or preprocessed data y_{Pr}^i) and the basis function x_1 are plotted in Fig. 3(g) and (h) for an active channel (Ch. 4), and in Fig. 3(i) and (j) for an inactive channel (Ch. 11). It is noteworthy that the estimated output variable $\hat{y}^i$ provides most of the adaptively preprocessed information consisting of baseline, and

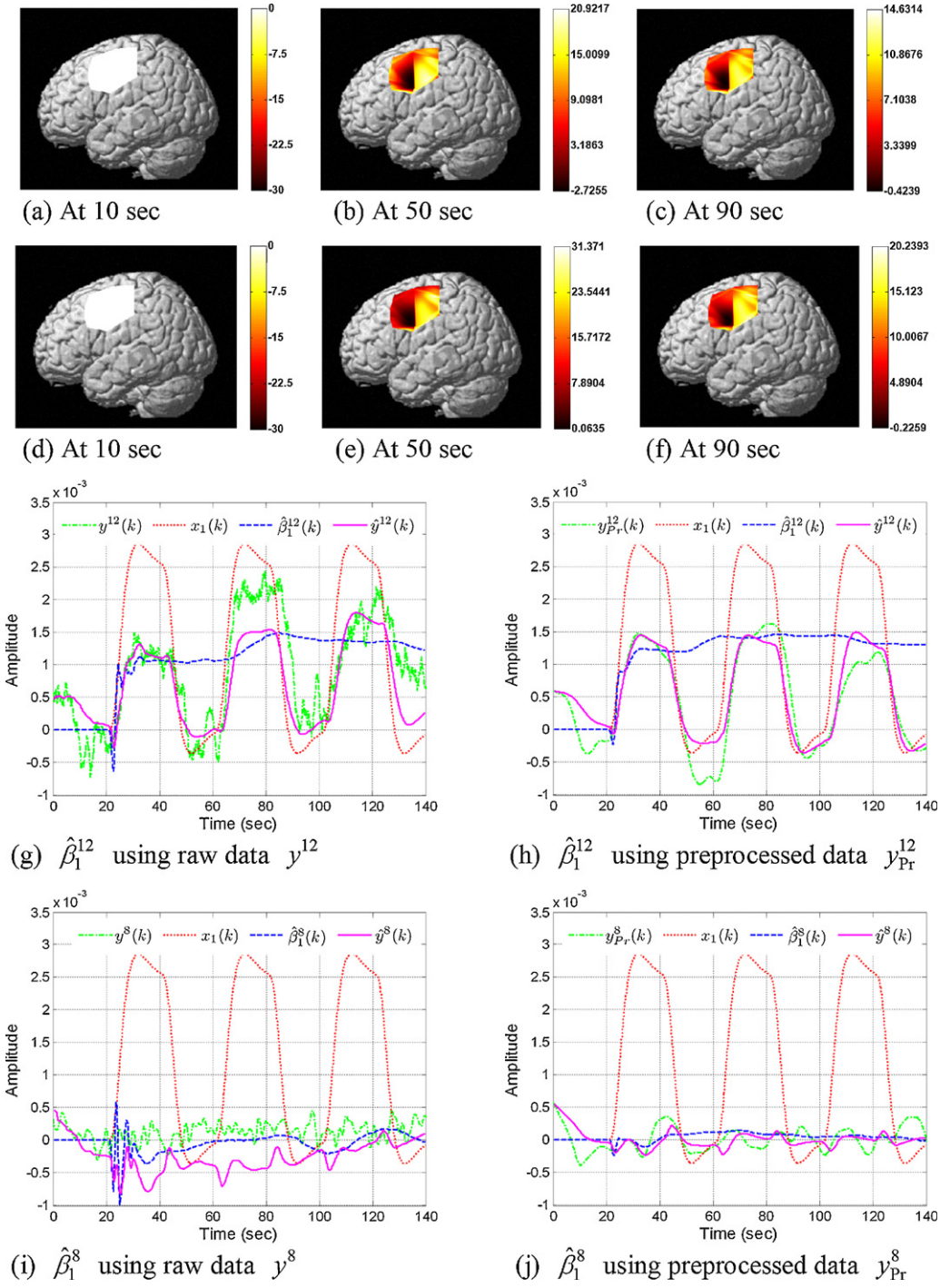

Fig. 4. Results with Imagent: (a)–(c) online brain activation maps obtained using raw data, (d)–(f) offline brain activation maps obtained using preprocessed data, (g) and (h) parameter convergence in an active channel (Ch. 12) (raw vs. preprocessed), and (i) and (j) parameter convergence in an inactive channel (Ch. 8) (raw vs. preprocessed).

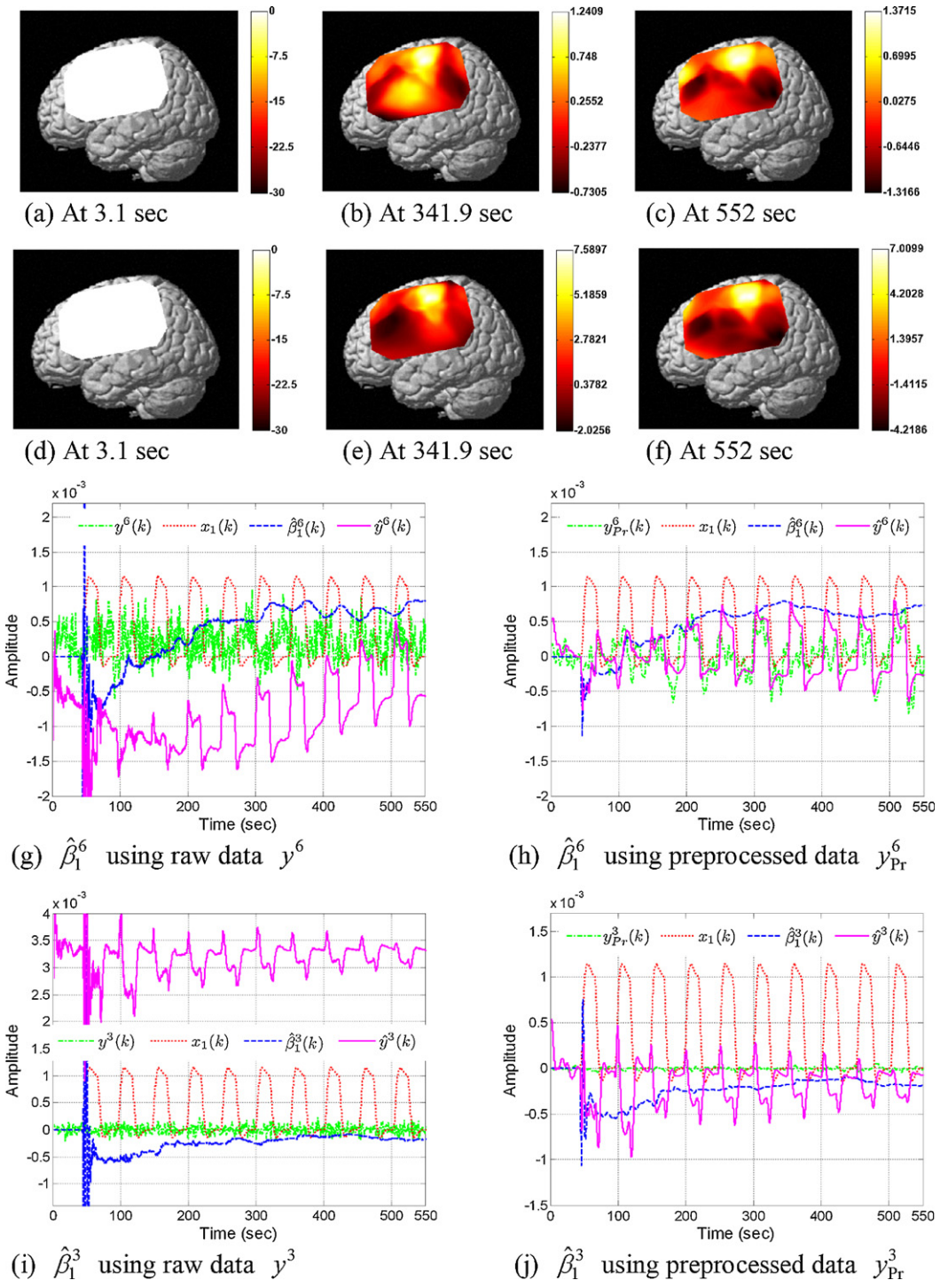

Fig. 5. Results with Oxymon: (a)–(c) online brain activation maps obtained using raw data, (d)–(f) offline brain activation maps obtained using preprocessed data, (g) and (h) parameter convergence in an active channel (Ch. 6) (raw vs. preprocessed), and (i) and (j) parameter convergence in an inactive channel (Ch. 3) (raw vs. preprocessed).

temporal trends of noise (whitening and/or coloring) of the specific channel i without affecting the estimation variable. It is apparent that each channel has its own status based on its location, placement, and motor alignment. Thus, the proposed methodology provides a robust treatment as per the respective channel requirements. Consistent results were obtained at all of the measuring channels.

Fig. 4(a)–(c) shows the online brain activation maps, using the Imagent probing instrument and its raw data, at three time instants 10, 50, and 90 s, respectively. Similarly to Fig. 3(d)–(f), Fig. 4(d)–(f) depict the brain activation maps obtained using preprocessed data. The parameter convergence plots are drawn in Fig. 4(g) and (h) for an active channel (Ch. 12), and in Fig. 4(i) and (j) for an inactive channel (Ch. 8). The almost identical results with raw and with preprocessed data demonstrate the robustness of the proposed RLSE approach for this instrument as well. Consistent results were obtained from all the dataset which were acquired twice with both CW- and FD-NIRS instruments from five subjects. Only small variations were observed in active channel locations and activity strengths. Such small discrepancies are due to channel misalignment during sensor fixation, varied attentiveness, and anatomical differences of individual subjects.

5. Discussion

The current study demonstrates the real-time brain-imaging capability of the proposed methodology with robustness by considering (but not restricting to) a canonical hemodynamic HbO response function. The proposed method can be extended to capture a broader range of phenomenology (like vascular steal, oxygen supply-demand imbalance [24], cerebral blood flow, cerebral blood volume, and oxygen saturation) to effectively address the voxel-to-voxel and subject-to-subject variability of the hemodynamic responses to neuroactivation.

The interpolation function $B(r)$ in (13) is supposed to be three-dimensional in a real measurement scenario. But, for optode-coverage manifold of current fNIRS probing, the two-dimensional interpolation function was sufficient to represent the interpolated fNIRS signals [25].

It should be noted that besides obviating the usual preprocessing steps, the method does not require pre-whitening or pre-coloring either. The validation against preprocessing, especially against pre-whitening and pre-coloring, was further confirmed by utilizing the block-design finger-tapping data made available in [25], which had been acquired with a different NIRS instrument (Oxymon MK III; Artinis). The dataset was obtained at 24 channels with behavioral protocol of an initial 42 s for signal equilibrium followed by ten repetitions of 21 s RIFT alternated with 30 s rest periods. Brain activation maps were drawn in Fig. 5(a)–(c) with raw data and in Fig. 5(d)–(f) with preprocessed data for selected sample times. It is noteworthy that the proposed result in Fig. 5(c), drawn after the convergence of activity parameters, is consistent with the offline result of [25] with all preprocessing including pre-coloring of the same dataset. The brain-mapping template (left lateral view) was depicted using the open-source software NIRS-SPM that was made available in [25] in order to effectively compare the results with their offline strategy. Such t-mapping can be drawn to any brain template by proper channel registration with reference points. Fig. 5(g and h) and (i and j) shows a closer look at the adaptive parameter convergence with robustness at the most activated channel 6 and at the inactivated channel 3, respectively, for the raw and preprocessed data.

6. Conclusions

This paper presented an RLSE-based framework for online brain imaging. The robust adaptive potential of the proposed approach provided a spatially adaptive preprocessing operation besides activity strength estimation. The validation was carried out by means of run-time experiments with CW- and FD-NIRS probing instruments. The methodology was further validated with the dataset in [25]. The scheme provided similar results with raw data and preprocessed data, demonstrating the robustness of the adaptive processing framework.

Acknowledgments

This research was supported by the World Class University program funded by the Ministry of Education, Science and Technology through the National Research Foundation of Korea (grant no. R31-20004).

References

[1] A.F. Abdelnour, T. Huppert, Real-time imaging of human brain function by near-infrared spectroscopy using an adaptive general linear model, NeuroImage 46 (2009) 133–143.
[2] M. Aqil, K.-S. Hong, M.-Y. Jeong, Synchronization of coupled chaotic FitzHugh–Nagumo systems, Commun. Nonlinear Sci. Numer. Simulat. 17 (2011) 1615–1627.
[3] D.A. Boas, M.A. O'Leary, B. Chance, A.G. Yodh, Detection and characterization of optical inhomogeneities with diffuse photon density waves: a signal-to-noise analysis, Appl. Opt. 36 (1997) 75–92.
[4] M. Cope, D.T. Delpy, System for long-term measurement of cerebral blood and tissue oxygenation on newborn-infants by near infra-red trans-illumination, Med. Biol. Eng. Comput. 26 (1988) 289–294.
[5] X. Cui, S. Bray, D.M. Bryant, G.H. Glover, A.L. Reiss, A quantitative comparison of NIRS and fMRI across multiple cognitive tasks, NeuroImage 54 (2011) 2808–2821.
[6] X. Cui, S. Bray, A.L. Reiss, Speeded near infrared spectroscopy (NIRS) response detection, PLoS One 5 (2010) e15474.
[7] A.J. den Dekker, D.H.J. Poot, R. Bos, J. Sijbers, Likelihood-based hypothesis tests for brain activation detection from MRI data disturbed by colored noise: A simulation study, IEEE Trans. Med. Imaging 28 (2009) 287–296.
[8] S. Fantini, D. Hueber, M.A. Franceschini, E. Gratton, W. Rosenfeld, P.G. Stubblefield, D. Maulik, M.R. Stankovic, Non-invasive optical monitoring of the newborn piglet brain using continuous-wave and frequency-domain spectroscopy, Phys. Med. Biol. 44 (1999) 1543–1563.
[9] K.J. Friston, J.T. Ashburner, S.J. Kiebel, T.E. Nichols, W.D. Penny, Statistical Parametric Mapping: The Analysis of Functional Brain Images, Academic Press, San Diego, 2008.
[10] S.S. Haykin, Adaptive Filter Theory, third ed., Prentice Hall, New Jersey, 2001.
[11] R.W. Homan, J. Herman, P. Purdy, Cerebral location of international 10–20 system electrode placement, Electroencephalogr. Clin. Neurophysiol. 66 (1987) 376–382.
[12] K.-S. Hong, Asymptotic behavior analysis of a coupled time-varying system: application to adaptive systems, IEEE Trans. Autom. Control 42 (1997) 1693–1697.
[13] X.-S. Hu, K.-S. Hong, S.S. Ge, Recognition of stimulus-evoked neuronal optical response by identifying chaos levels of near-infrared spectroscopy time series, Neurosci. Lett. 504 (2011) 115–120.
[14] X.-S. Hu, K.-S. Hong, S.S. Ge, M.-Y. Jeong, Kalman estimator- and general linear model-based on-line brain activation mapping by near-infrared spectroscopy, Biomed. Eng. Online 9 (2010) 82.
[15] H. Ichikawa, S. Kanazawa, M.K. Yamaguchi, R. Kakigi, Infant brain activity while viewing facial movement of point-light displays as measured by near-infrared spectroscopy (NIRS), Neurosci. Lett. 482 (2010) 90–94.
[16] P. Liu, G.Y. Zhou, Y. Zhang, M.H. Dong, W. Qin, K. Yuan, J.B. Sun, J.X. Liu, J.M. Liang, K.M. von Deneen, Y.J. Liu, J. Tian, The hybrid GLM-ICA investigation on the neural mechanism of acupoint ST36: an fMRI study, Neurosci. Lett. 479 (2010) 267–271.
[17] G.H. Lu, J.S. Brittain, P. Holland, J. Yianni, A.L. Green, J.F. Stein, T.Z. Aziz, S.Y. Wang, Removing ECG noise from surface EMG signals using adaptive filtering, Neurosci. Lett. 462 (2009) 14–19.
[18] M. Okamoto, H. Dan, K. Sakamoto, K. Takeo, K. Shimizu, S. Kohno, I. Oda, Three-dimensional probabilistic anatomical cranio-cerebral correlation via the international 10–20 system oriented for transcranial functional brain mapping, NeuroImage 21 (2004) 99–111.
[19] M. O'Leary, D. Boas, B. Chance, A. Yodh, Experimental images of heterogeneous turbid media by frequency-domain diffusing-photon tomography, Opt. Lett. 20 (1995) 426–428.
[20] M.M. Plichta, S. Heinzel, A.C. Ehlis, P. Pauli, A.J. Fallgatter, Model-based analysis of rapid event-related functional near-infrared spectroscopy (NIRS) data: a parametric validation study, NeuroImage 35 (2007) 625–634.
[21] A. Tachibana, J.A. Noah, S. Bronner, Y. Ono, M. Onozuka, Parietal and temporal activity during a multimodal dance video game: an fNIRS study, Neurosci. Lett. 503 (2011) 125–130.
[22] A. Villringer, U. Dirnafl, Coupling of brain activity and cerebral blood flow: basis of functional neuroimaging, Cerebrovasc. Brain Metab. Rev. 7 (1995) 240–276.
[23] N. Weiskopf, R. Sitaram, O. Josephs, R. Veit, F. Scharnowski, R. Goebel, N. Birbaumer, R. Deichmann, K. Mathiak, Real-time functional magnetic resonance imaging: methods and applications, Magn. Reson. Imaging 25 (2007) 989–1003.
[24] G.R. Wylie, H.L. Graber, G.T. Voelbel, A.D. Kohl, J. DeLuca, Y. Pei, Y. Xu, R.L. Barbour, Using co-variations in the Hb signal to detect visual activation: a near infrared spectroscopic imaging study, NeuroImage 47 (2009) 473–481.
[25] J.C. Ye, S.H. Tak, K.E. Jang, J.W. Jung, J.D. Jang, NIRS-SPM: statistical parametric mapping for near-infrared spectroscopy, NeuroImage 44 (2009) 428–447.